Coupled Analysis of Navier-Stokes and Darcy Flows by the Brinkman Equations

S. Arimoto[1], K. Fujisawa[1] and A. Murakami[1]
[1]*Graduate School of Agriculture, Kyoto-Univeersity, Kyoto, Japan*
E-mail: ant_book@yk.commufa.jp

ABSTRACT: Simultaneous analysis of seepage flows in porous media and regular flows in fluid domains has a variety of applications to practical problems. The objective of this paper is to present a numerical method to simulate these two different flows simultaneously and continuously, and to investigate the influence of the Darcy flows in porous media on the Navier-Stokes flows in the fluid domain. To this end, the authors have employed the Darcy-Brinkman equations, which include the Navier-Stokes equations and can approximately describe Darcy flows by changing the values of porosity and hydraulic conductivity. The solutions of the Darcy-Brinkman equations are affected by two dimensionless quantity, i.e., the Reynolds number, Re and the Darcy number, Da. After the procedures to provide stable solutions of the governing equations are explained, this paper considers the two types of problems involving Navier-Stokes/Darcy coupled flows and the influence of the two dimensionless parameters on the solutions are investigated. One is the backward-facing step flow with a porous step, and the other is the preferential flows in porous media. The numerical results have shown that the permeability of the porous step slightly affects the reattachment of the flow in the former problem, and that the shape of the void or cavity in porous media changes the structure of the flow in it and the Darcy number changes the flux into the fluid domain in the latter problem.

KEYWORDS: Darcy's law, Navier-Stokes equations, Coupled analysis, Darcy-Brinkman equations.

1. INTRODUCTION

The simultaneous computation of seepage flows in porous media and regular flows in fluid domains has a variety of applications to practical problems related to the prevention of natural disasters, such as the erosion of soil structures, piping flows within natural slopes, and the stability of embankments subjected to tidal waves. For example, the erosion of soils is affected by surface flows as well as by subsurface flows, i.e., seepage flows, and these two flow fields need to be grasped in order to predict how the erosion develops. This paper concentrates on the water flows through these two domains and proposes a numerical method to compute the two flow fields simultaneously.

The studies about the interaction of Navier-Stokes and seepage flow in fluid domain can be traced to the velocity on boundary between the fluid and the Darcy phases. Beavers and Joseph (1967) experimented in Hagen-Poiseuille flow which was in a condition of seepage flow occurring along a wall, and discussed the boundary conditions of the fluid domain. On the ground of their experiment results, they suggested that it was desirable to give slip condition to boundary between the fluid and the Darcy phases. After that, components of flow velocity along boundary of between the fluid and the Darcy phases were discussed several times. Saffman (1971) improved the model which was proposed by Beavers and Joseph (1967). Moreover, Neale and Nader (1974) explained velocity and stress on boundary between the fluid and the Darcy phases using the continuous model. In addition, Bars and Worster (2006), Ochoa-Tapia and Whitaker (1995a, 1995b) were also discussed. A great deal of effort has been made on this problem, the best model has not be obtained. Thus far, there have been several numerical studies dealing with the coupled analysis of the Navier-Stokes and the Darcy flows (e.g., Girault & Rivière, 2009; Cai et al., 2009). They adopted different governing equations between the fluid and the Darcy phases, as shown in Eq. (1) and (2);

$$\frac{\partial u_i}{\partial x_i} = 0 \tag{1a}$$

$$\frac{\partial u_i}{\partial t} + \frac{\partial u_i u_j}{\partial x_j} = -\frac{1}{\rho}\frac{\partial p}{\partial x_i} + \nu \frac{\partial^2 u_i}{\partial x_j \partial x_j} \tag{1b}$$

$$\frac{\partial}{\partial x_i}\left(\frac{k}{\rho g}\frac{\partial p}{\partial x_i}\right) = 0 \tag{2}$$

where u_i, p, ρ, ν, k and g denote the flow velocity, the piezometric pressure, the density of water, the kinematic viscosity of water, the hydraulic conductivity and the gravitational acceleration, and t and x_i are time and Cartesian coordinates. Girault & Rivière (2009) numerically analyzed the steady solutions of Eq. (1) and (2) by the discontinuous Galerkin scheme, and Chidyagwai & Rivière (2009) discussed the existence and uniqueness of the numerical solutions which are discontinuous at the interface between the Darcy and the fluid domain. Badea et al.(2010) implemented coupling of the fluid and the Darcy phases using the iterative method, and Chidyagwai & Rivière (2011), Cai et al.(2009), Mu & Xu (2007) proposed the numerical schemes to solve Eq. (1) and (2) using the Two Grid Method, which can reduce the computational cost with the aid of coarse and fine grids. Çeşmelioğlu and Rivière (2012) started studies about existence of solutions in a problem which was coupled with advection-diffusion equation in addition to Eq. (1) and (2). Their interest is mainly in the mathematical treatment used to connect the numerical solutions in the two different phases, and the numerical procedure for satisfying the conservation of mass and momentum at the interface is not as easy as is applicable to practical problems. The objective of this article is to propose a simple numerical method to simultaneously solve the Navier-Stokes and the Darcy flows, which is uncomplicated and applicable to the practical problems.

2. GOVERNING EQUATIONS

The following partial differential equations, called Darcy-Brinkman equations, are employed for the coupled analysis of the Navier-Stokes flow in the fluid domain and the Darcy flow in porous media.

$$\frac{\partial u_i}{\partial x_i} = 0 \tag{3a}$$

$$\frac{\partial u_i}{\partial t} + \frac{\partial}{\partial x_j}\left(\frac{u_i u_j}{\lambda}\right) = -\frac{\lambda}{\rho}\frac{\partial p}{\partial x_i} + \nu \frac{\partial^2 u_i}{\partial x_j \partial x_j} - \frac{\lambda g}{k} u_i \tag{3b}$$

where λ denotes the porosity. The flow velocity u_i in Eq. (3) means the usual flow velocity in the fluid domain and the Darcy velocity in porous media. The Darcy-Brinkman equations can be derived by taking the volume-average of the Navier-Stokes equations over the domain of porous media and the concise derivation is seen in Bars &

Worster (2006). It can be easily understood that Eq. (3) becomes the Navier-Stokes equations, when λ =1.0 and $1/k$=0 are given.

The non-dimensionalization of Eq. (3) reveals that two types of dimensionless parameters, i.e., the Reynolds and the Darcy numbers, affect its solutions. Introducing the non-dimensional quantities of u_i^+, x_i^+ and t^+ as follows;

$$u_i = Vu_i^+ \,,\; x_i = Lx_i^+ \,,\; t = \frac{L}{V}t^+ \tag{4}$$

and substituting Eq. (4) into Eq. (3), it can be reduced into the following form;

$$\frac{\partial u_i^+}{\partial x_i^+} = 0 \tag{5a}$$

$$\mathrm{Re}\left[\frac{\partial u_i^+}{\partial t^+} + \frac{\partial}{\partial x_j^+}\left(\frac{u_i^+ u_j^+}{\lambda}\right)\right] = -\lambda \frac{L}{\rho \nu V}\frac{\partial p}{\partial x_i^+} + \frac{\partial^2 u_i^+}{\partial x_j^+ \partial x_j^+} - \lambda \mathrm{Da}^{-1} u_i^+ \tag{5b}$$

where Re and Da denote the Reynolds and the Darcy numbers, respectively. The dimensionless numbers are defined as follows.

$$\mathrm{Re} = \frac{VL}{\nu} \,,\; \mathrm{Da} = \frac{k\nu}{gL^2} \tag{6}$$

The first term in the right hand sided of Eq. (5b) is not fully nondimensionalized because the nondimensionalization of the pressure depends on whether the fluid domain or the porous media are taken into consideration. In the fluid domain, the pressure can be nondimensionalized by $p = \rho V^2 p^+$, because the pressure depends on the change of velocity head. Substituting $p = \rho V^2 p^+$ into Eq. (5b), it is reduced into the following form;

$$\mathrm{Re}\left[\frac{\partial u_i^+}{\partial t^+} + \frac{\partial}{\partial x_j^+}\left(\frac{u_i^+ u_j^+}{\lambda}\right)\right] = -\lambda\, \mathrm{Re} \frac{\partial p^+}{\partial x_i^+} + \frac{\partial^2 u_i^+}{\partial x_j^+ \partial x_j^+} - \lambda \mathrm{Da}^{-1} u_i^+ \tag{7}$$

In the fluid domain, λ =1.0 and $1/k$=0 (Da^{-1}=0) hold true and Eq. (7) becomes the nondimensional Navier-Stokes equations. On the other hand, the pressure changes with the loss of hydraulic head in porous media. Hence, the pressure can be nondimensionalized by $p = \rho gLVp^+/k$, noting that V/k means the representative hydraulic gradient. Substituting $p = \rho gLVp^+/k$ into Eq. (5b), it is rewritten into the following form;

$$\mathrm{Re}\left[\frac{\partial u_i^+}{\partial t^+} + \frac{\partial}{\partial x_j^+}\left(\frac{u_i^+ u_j^+}{\lambda}\right)\right] = -\lambda \mathrm{Da}^{-1} \frac{\partial p^+}{\partial x_i^+} + \frac{\partial^2 u_i^+}{\partial x_j^+ \partial x_j^+} - \lambda \mathrm{Da}^{-1} u_i^+ \tag{8}$$

When the hydraulic conductivity is sufficiently small and the inverse of the Darcy number Da^{-1} is even larger than the Reynolds number, i.e., $\mathrm{Da}^{-1} \gg \mathrm{Re}$ and Da^{-1}=1, the left hand side and the second term of the right hand side of Eq. (8) becomes negligible. Then, Eq.(8) can be transformed into the following form:

$$\frac{\partial p^+}{\partial x_i^+} + u_i^+ = 0 \tag{9}$$

Eq. (9) is identical to the well-known Darcy's law, which implies that the Darcy's law is approximately described by the Darcy-Brinkman equations when the hydraulic conductivity is sufficiently small. Eq. (3) can describe the Navier-Stokes equations in the fluid domain by giving λ=1.0 and $1/k$=0, and can approximate the Darcy's law in porous media. Therefore, the Darcy-Brinkman equations allows us to simulate the Darcy and the Navier-Stokes flows without employing the different governing equations in the fluid domain and the porous media. It should be noted that the solution of the Darcy-Brinkman equations depends on both the Reynolds number Re and the Darcy number Da.

3. NUMERICAL METHOD

3.1 Characteristics

A numerical method to solve the Darcy-Brinkman equations of Eq. (3) was proposed by Fujisawa et al. (2013). Their method based on the one proposed by Kim & Choi (2000), which can solve the Navier-Stokes equations for incompressible fluids by the finite volume method with unstructured grids. The method is characterized by the grid system shown in Figure 1. The velocity and the pressure are stored at the centroids of the finite volume cells and the flux U is additionally computed at the mid-point of each cell face, which has the following definition;

$$U = (u_i)_{\mathrm{face}} n_i \tag{10}$$

where $(u_i)_{\mathrm{face}}$ and n_i denote the flow velocity and outward-normal unit vector on the cell face, respectively.

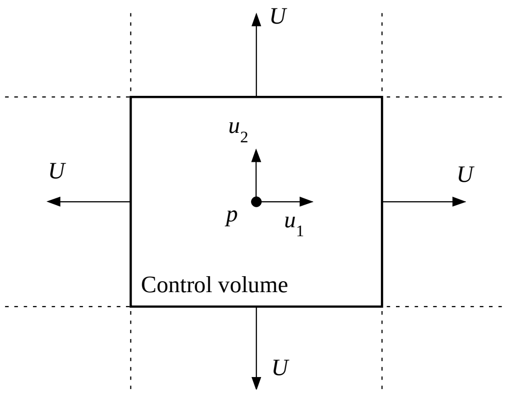

Figure 1 Finite volume cells and variables

The advantages of the method for the simultaneous analysis of the Navier-Stokes and the Darcy flows are summarized as follows.

1. The finite volume discretization can definitely divide the Darcy phase with the fluid domain, unlike the finite difference method.
2. The usage of the flux U defined at the cell faces enables the conservation of mass and momentum to be satisfied at the interface between the fluid domain and porous media.
3. The finite volume method allows the variables at the cell faces to be freely constructed unlike the common finite element method. This is advantageous for extending the numerical method. For example, the discontinuous tangential flow velocity at the interface between the two different domains (e.g., Beavers & Joseph, 1967) and be easily introduced, although the flow velocity is continuously interpolated herein for simplicity.

The method proposed by Kim & Choi (2000) for numerically solving the Navier-Stokes equations can accept the unstructured grids. However, the usage of the unstructured grids is not straightforward when there exist the two different domains, i.e., the fluid and porous domains. Hence, the structured grid is employed in the following formulations and numerical simulations in this paper.

3.2 Numerical procedures

The numerical procedures for the rectangular finite volume cells shown in Figure 1 are presented in this section. A fractional step method is applied to Eq. (3): The flow velocity is predicted by Eq. (3b), and then the predicted flow velocity is corrected so as to satisfy the continuity equation of Eq. (3a). When the flow velocity is predicted by Eq. (3b), Eq. (3b) is divided into following two steps;

$$\frac{\partial u_i}{\partial t} = -\frac{\lambda g}{k} u_i \tag{11}$$

$$\frac{\partial u_i}{\partial t} = -\frac{\partial}{\partial x_j}\left(\frac{u_i u_j}{\lambda}\right) - \frac{\lambda}{\rho}\frac{\partial p}{\partial x_i} + \nu \frac{\partial^2 u_i}{\partial x_j \partial x_j} \tag{12}$$

Applying the fractional step method and the Crank–Nicolson method to the time integration of Eqs. (11) and (12), Eqs. (13) to (17) can be derived;

$$\frac{u_i' - u_i^m}{\Delta t} = -\frac{\lambda g}{2k}\left(u_i' + u_i^m\right) \tag{13}$$

$$\frac{\hat{u}_i - u_i'}{\Delta t} = -\frac{1}{2}\frac{\partial}{\partial x_j}\left(\frac{\hat{u}_i u_j^m + u_i^m \hat{u}_j}{\lambda}\right) - \frac{\lambda}{\rho}\frac{\partial p^m}{\partial x_i} + \frac{\nu}{2}\frac{\partial^2}{\partial x_j \partial x_i}\left(\hat{u}_i + u_i^m\right) \tag{14}$$

$$\frac{u_i^* - \hat{u}_i}{\Delta t} = \frac{\lambda}{\rho}\frac{\partial p^m}{\partial x_i} \tag{15}$$

$$\frac{\partial}{\partial x_j}\left(\frac{\lambda}{\rho}\frac{\partial p^{m+1}}{\partial x_j}\right) = \frac{1}{\Delta t}\frac{\partial u_j^*}{\partial x_j} \tag{16}$$

$$\frac{u_i^{m+1} - u_i^*}{\Delta t} = -\frac{\lambda}{\rho}\frac{\partial p^{m+1}}{\partial x_i} \tag{17}$$

where u_i', $\hat{u}_i$ and u_i^* denote the intermediate velocities between u_i^m and u_i^{m+1}, respectively, and Δt is the size of time steps. The superscript m implies the iteration for the time steps. u_i' is the intermediate velocity calculated by Eq. (11) and $\hat{u}_i$ is obtained from the integration of Eq. (12) using u_i' for the initial value. Eqs. (13) and (14) correspond to the prediction step of the flow velocity, and Eqs. (15) to (17) conduct the calculation of the pressure and the correction of the predicted flow velocity to satisfy the continuity equation. Integrating Eqs. (13) to (17) over the finite volume cells, and applying the Gauss divergence theorem, Eqs. (13) to (17) are transformed into

$$\frac{u_i' - u_i^m}{\Delta t} = -\frac{\lambda g}{2k}\left(u_i' + u_i^m\right) \tag{18}$$

$$\begin{aligned}\frac{\hat{u}_i - u_i'}{\Delta t} &= -\frac{1}{A}\oint_l \frac{1}{2\lambda}\left(\hat{u}_i U^m + u_i^m \hat{u}_j n_j\right) dl \\ &\quad - \frac{1}{A}\cdot\frac{\lambda}{\rho}\oint_l p^m n_i dl + \frac{1}{A}\cdot\frac{\nu}{2}\oint_l \frac{\partial}{\partial n}\left(\hat{u}_i + u_i^m\right) dl\end{aligned} \tag{19}$$

$$\frac{u_i^* - \hat{u}_i}{\Delta t} = \frac{1}{A}\cdot\frac{\lambda}{\rho}\int_l p^m n_i dl \tag{20}$$

$$\oint_l \frac{\lambda}{\rho}\frac{\partial p^{m+1}}{\partial n} dl = \frac{1}{\Delta t}\oint_l U^* dl \tag{21}$$

$$\frac{u_i^{m+1} - u_i^*}{\Delta t} = -\frac{1}{A}\cdot\frac{\lambda}{\rho}\oint_l p^{m+1} n_i dl \tag{22}$$

$$\frac{U^{m+1} - U^*}{\Delta t} = -\frac{\lambda}{\rho}\frac{\partial p^{m+1}}{\partial n} \tag{23}$$

where A, l and n_i denote the area of the cell, the length of the cell faces, the outward normal unit vector at the cell faces, respectively, and $\partial/\partial n$ implies the directional derivative for the outward normal direction. The porosity λ is constant in each finite volume cell. U is the flux defined at each cell face and Eq. (23) is derived by multiplying n_i with Eq. (17). U^* ($= u_i^* n_i$) is the intermediate flux and is calculated using Eq. (10), interpolating the intermediate velocity u_i^* at the centroids of each cell to the cell faces. The method for the interpolation of the velocity and the pressure to the cell faces is explained in Appendix A. Substituting Eq. (23) into Eq. (21), following equality is obtained;

$$\oint_l U^{m+1} dl = 0 \tag{24}$$

Eq. (24) means that the velocity at each finite volume cells satisfies the continuity equation.

3.3 Interpolation of velocity and pressure

In order to compute the integrals appearing in Eq. (18) to (22) and to discretise these equations, the velocities, the pressure and their directional derivatives need to be evaluated at the mid-point of each cell face. The values of the velocities and the pressure, except for the flux U, are stored at the centroids of the finite volume cells (See Figure 1), and they need to be interpolated at each cell face from those at the centroids of neighboring cells. Then, the manner of interpolating these variables plays an important role in the stable computation at the interface between the Darcy and the Fluid domains. If the simple linear interpolation scheme proposed by Kim & Choi (2000) is applied to the coupled analysis of Darcy and Navier-Stokes flows, the physically unrealistic oscillations appear at the interface between the Fluid and the Darcy Phase. Fujisawa et al. (2013) proposed the improved interpolation scheme which can avoid the oscillation. The details of the proposed the improved interpolation scheme is explained in Appendix A. This improved interpolation scheme is used in the several numerical computation presented in this article.

3.4 Linear solvers

Eqs. (19) and (21) become the systems of linear equations for the velocity $\hat{u}_i$ and the pressure p^{m+1}, respectively. Letting N_c be the total number of the finite volume cells, Eq. (19) produces a $2Nc \times 2Nc$ matrix, and Eq. (21) does $Nc \times Nc$. Generally, these matrixes are asymmetric and sparse. The Gauss-Seidel method was used for Eq. (19), and QMRCGSTAB method (Chan et al., 1994), which is a variant of the BiCG method, was applied to Eq. (21).

4. NUMERICAL RESULTS

4.1 Backward-facing step flow with a porous medium

The backward-facing step flow with a porous medium was computed by the numerical method presented in the previous chapter. The geometry and the boundary conditions of the problem is shown in Figure 2. The porous medium was installed as the backward-facing step and located in the bottom left of the computational domain. The parabolic profile of the flow velocity was given onto the left boundary of the fluid domain and the right side had the free outflow condition where the pressure and the gradient of the velocity was zero. The non-slip condition was imposed onto the top and bottom sides. The flow velocity and the pressure were initially set to zero in all of computational domain. The finite volume cells are shown in Figure 3. Total 16,000 finite volume cells were used. The computation was carried out until the flow field became steady.

Varying the hydraulic conductivity of the porous medium and the inflow rate, how the reattachment point changes with the Reynolds number Re and the Darcy number Da was investigated. Re in this problem is defined as Re=$U_{ave}\ L\ /\ \nu$, where U_{ave} is the bulk velocity in the fluid domain and L is the height of the channel (See Figure 2). Three different Reynolds numbers of 264, 396 and 528 were assumed, and these values were placed in the rage of the previous studies of the backward-facing step flow (e.g., Kim & Moin 1985; Kim & Choi, 2000). The velocity distributions at the steady state are shown in Figures 4 to 6. In these figures, Re is fixed as 528 and Da has three different values of 1.0×10^{-11}, 1.0×10^{-7}, and 1.0×10^{-3}.

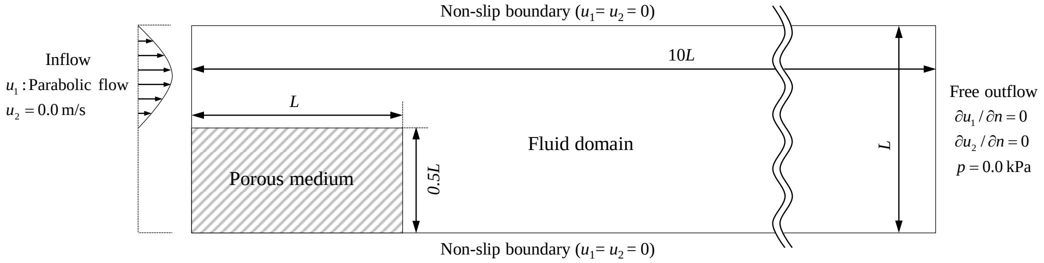

Figure 2 Geometry and boundary conditions

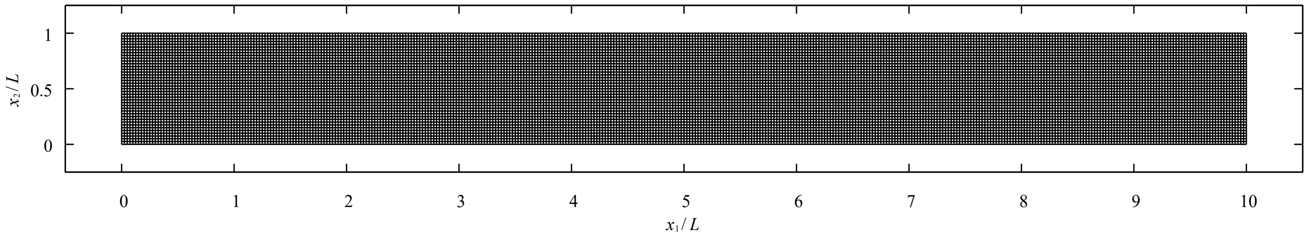

Figure 3 Computational finite volume cells for Backward-facing step flow

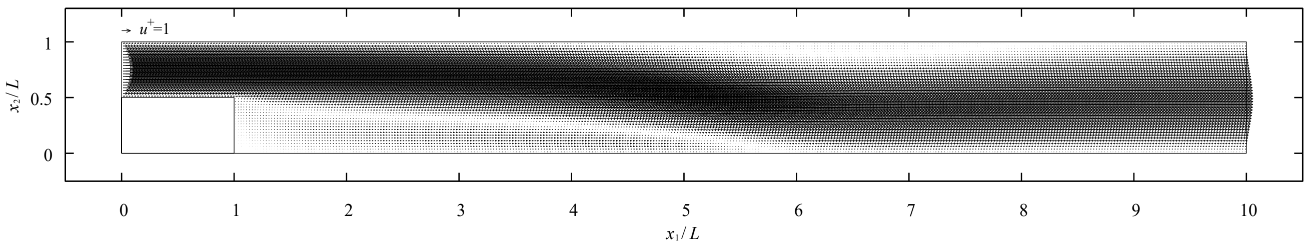

Figure 4 Computed velocity vector of flow (Re=528, Da=1.0×10^{-11})

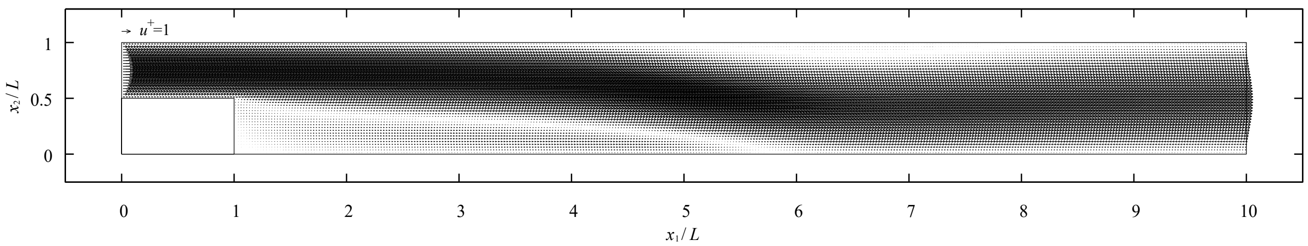

Figure 5 Computed velocity vector of flow (Re=528, Da=1.0×10^{-7})

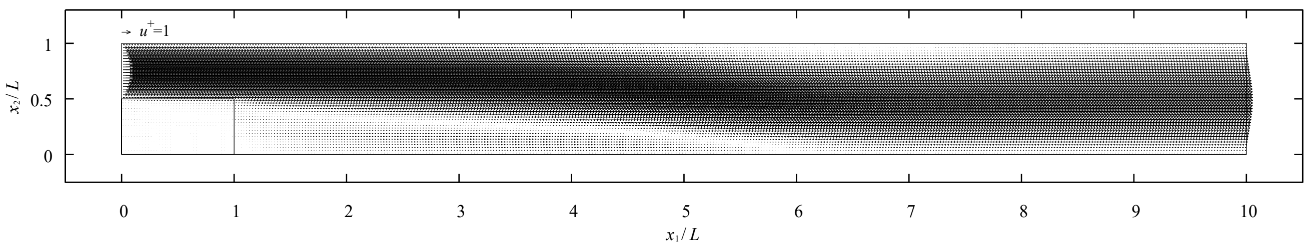

Figure 6 Computed velocity vector of flow (Re=528, Da=1.0×10^{-3})

The flows in the figures exhibit the separation bubble after the porous steps as is usually seen in the backward-facing step flow. Figure 7 shows the seepage flow velocity in the porous step when Da=1.0×10^{-3} was given. The flow velocity is greater around the upper surface. Figure 8 shows the relationship between Da and the position of reattachment point. In this figure, the reattachment point do not significantly changes even if Da varies from 1.0×10^{-11} to 1.0×10^{-3}. This is because the velocity in the porous medium is even smaller than that in the fluid domain as shown in Figure 9. However, in the case of Da=1.0×10^{-3}, the profile of the flow velocity at the edge of the step diverts from the Hagen-Poiseuille flow (See Figure 9), and the reattachment point moves slightly further from the step.

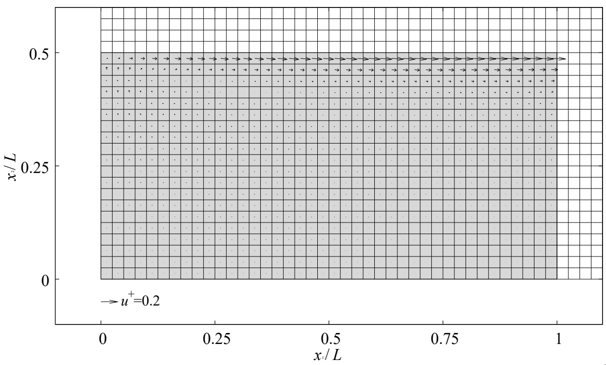

Figure 7 Velocity vector in porous step (Re=528, Da=1.0×10^{-3})

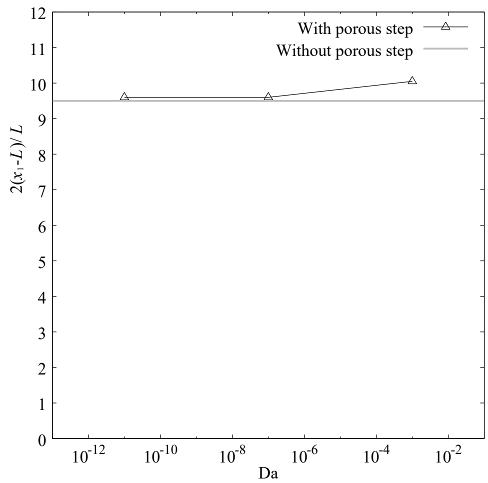

Figure 8 Plot of the reattachment point using the Darcy number (Re=528)

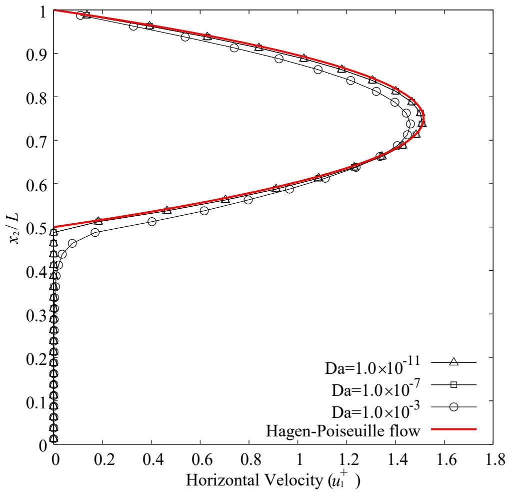

Figure 9 Distribution of velocity at vertical lines of x_1/L=1.0 (Re=528)

Figure 10 shows the relationship between Re and the positions of the reattachment point in two cases; one has the porous step (Da=1.0×10^{-3}) and the other is the regular backward-facing step flow with an impermeable step. The reattachment points computed in the two cases become closer to the step as the Reynolds number decreases, and the results are consistent with Kim and Moin (1985). These results indicate that the influence of Da on the position of reattachment point is small, because Re has a dominant influence on the flow in the fluid domain.

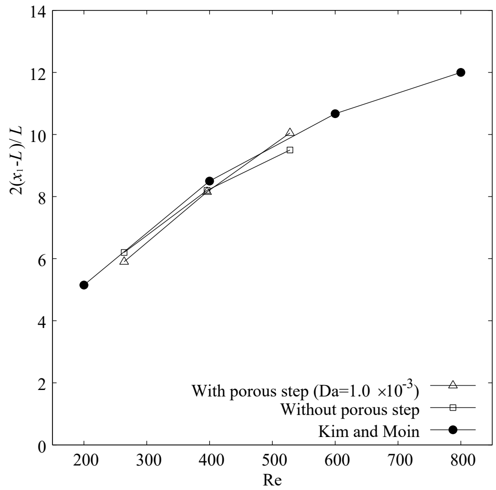

Figure 10 Plot of the reattachment point using the Reynolds number

4.2 Preferential flow within porous media

The seepage flows in a porous medium including a void were computed. Figure 11 shows the geometry and the boundary conditions of this problem. The computation was carried out in the rectangular domain. The domain was assumed to be filled with a porous media such as soil, and the void was located around the centre of the computational domain. Three different sizes of the void were prepared as seen in Table 1. Figures 12 to 14 show the finite volume cells of the three cases. Several cases with different values of Re and Da were computed. The porosity was assumed to be 0.40. The uniform inflow velocity was given to the left side of the computational domain, while the free outflow boundary condition was imposed onto the right side. Re and Da was controlled by the inflow velocity from the left side and the hydraulic conductivity of the porous medium. Re was selected in the range where laminar flows could be achieved in the void. Re is defined as Re=$U_{in}\,L\,/\,\nu$, where U_{in} is the velocity on the inflow boundary and L is the representative length of the domain (See Figure 11). Both the upper and lower sides had the free-slip boundary condition. Assuming the flow velocity and the pressure to be zero as the initial conditions, the numerical computation was conducted until the flow field reached the steady state. The Finite volume cells used in the numerical computation are shown in Figures 12 to 14.

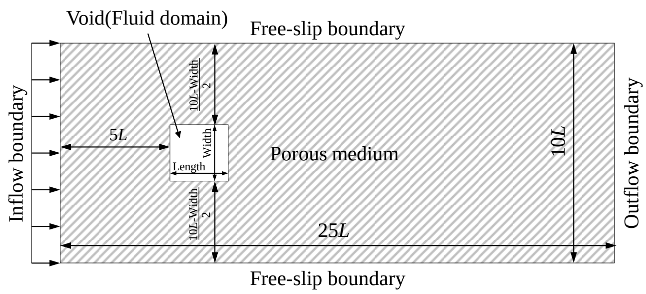

Figure 11 Geometry and boundary conditions

Table 1 Size and aspect ratio of void

Length	**Width**	**Aspect ratio** (=Length /Width)
4*L*	*L*	4.0
2*L*	2*L*	1.0
L	4*L*	0.25

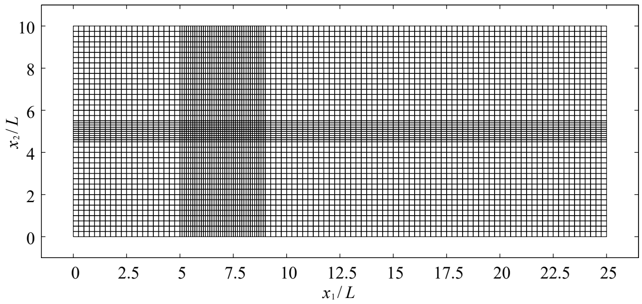

Figure 12 Computational finite volume cells (Aspect ratio=4.0)

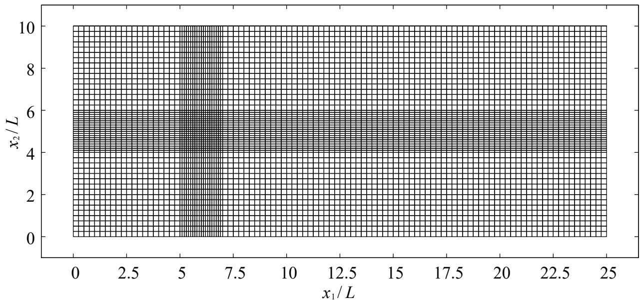

Figure 13 Computational finite volume cells (Aspect ratio=1.0)

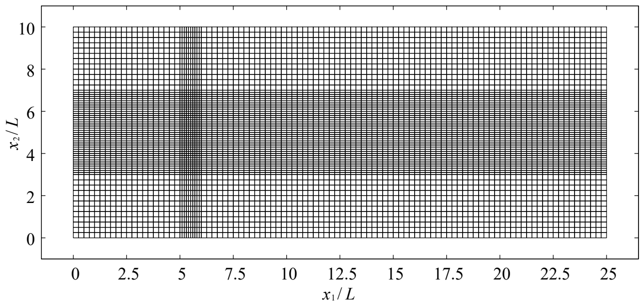

Figure 14 Computational finite volume cells (Aspect ratio=0.25)

Figures 15 to 17 show the flow velocity under the steady state. Water concentrates into the void and passes through it. When the aspect ratio is 1.0 or 0.25, the seepage water comes into the void from the corners of its left side, and forms the two major streams along the upper and lower side. On the other hand, when the aspect ratio is 4.0, the two streams in the left side of the void immediately combine and develop into a main steam.

Figure 18 shows the profiles of the horizontal flow velocity at the central cross section of the void. The velocity profile of aspect ratio=4.0 is almost parabolic. Moreover, the tangential velocity at the interface between the porous medium and the void became smaller in all cases, because the pressure in the void does not change significantly and the interface behaves as a constant pressure line. Figure 19 shows the velocity profile at the different cross section of the void when the aspect ratio is 4.0. It can be seen that the velocity profile quickly approaches to the parabolic shape although it is not parabolic at all in the left side of the void.

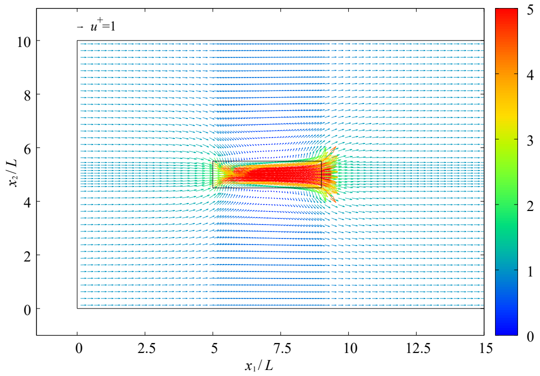

Figure 15 Computed velocity vector of flow (Aspect ratio=4.0, Re=30, Da=2.5×10^{-8})

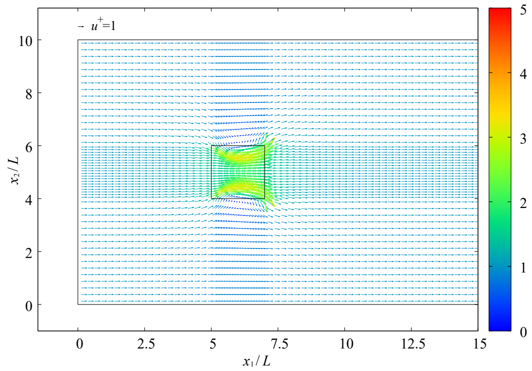

Figure 16 Computed velocity vector of flow (Aspect ratio=1.0, Re=30, Da=2.5×10^{-8})

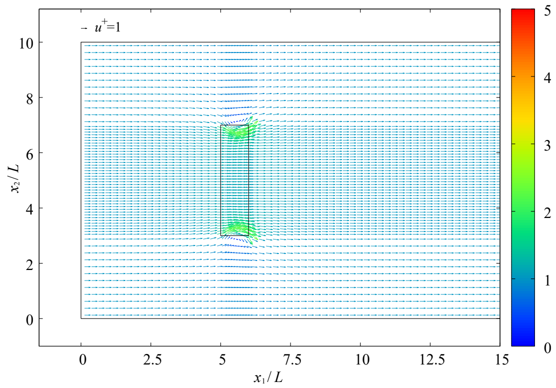

Figure 17 Computed velocity vector of flow (Aspect ratio=0.25, Re=30, Da=2.5×10^{-8})

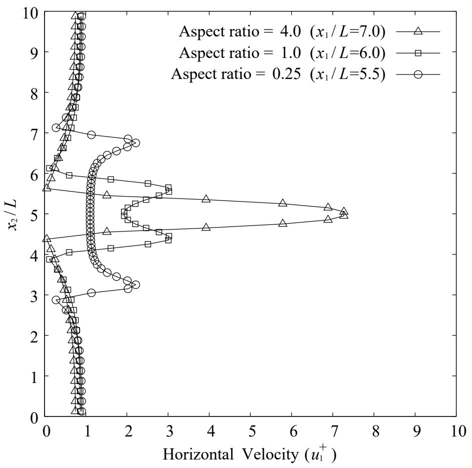

Figure 18 Distribution of horizontal velocity at the centre of the void (Re=30, Da=2.5×10^{-8})

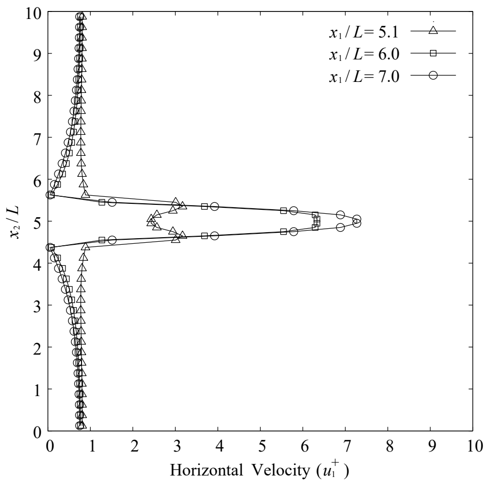

Figure 19 Distribution of horizontal velocity at x_1/L=5.1, 6.0 and 7.0 (Aspect ratio=4.0, Re=30, Da=2.5×10^{-8})

Figure 20 shows the relationship between the maximum velocity in the void and the aspect ratio. The maximum velocity increases with the increase of the aspect ratio. Figure 21 shows the influence of Re and Da on the maximum velocity. The maximum velocity depends on Da because the inflow/outflow velocity on the interface between the porous medium and the fluid domain changes as shown in Figure 22. U denoting the flux of Eq. (10) at the left and upper sides are exhibited in the figure, where the positive and negative values of U means inflow to and outflow from the void, respectively. The inflow velocity of Da=2.5×10^{-8} at the corners of the left side is greater than that of Da=2.5×10^{-4}, while the velocity of Da=2.5×10^{-8} on the upper side is smaller than that of Da=2.5×10^{-4}. Thus, in the case of Da=2.5×10^{-8}, the main stream in the void accelerates and reaches the maximum velocity around the centre of the void. On the other hand, the acceleration of the main stream of Da=2.5×10^{-4} is slower, because the inflow from the upper and lower sides decelerates the main stream (see Figure 23). Figure 24 shows the relationship between Re and the maximum velocity in case of Da=2.5×10^{-8}. The maximum velocities linearly increase with increasing Re, because Re is controlled by the inflow velocity and the patterns of flow in the void do not change.

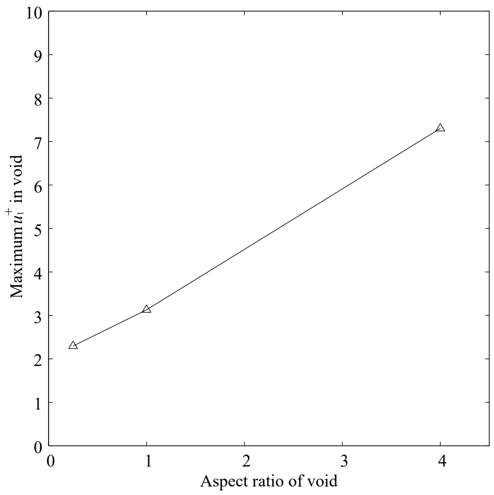

Figure 20 The relationship between maximum velocity in void and aspect ratio (Re=30, Da=2.5×10^{-8})

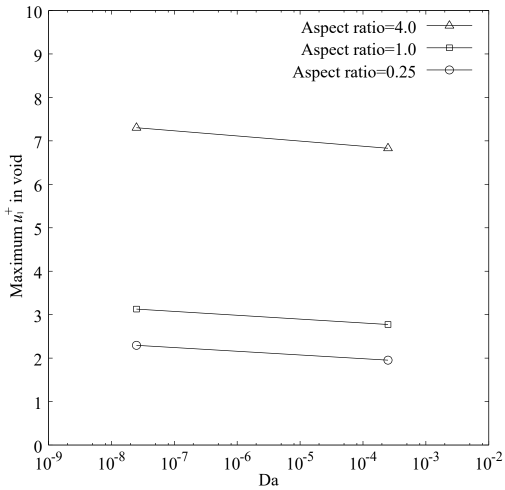

Figure 21 The relationship between maximum velocity and Da (Re=30)

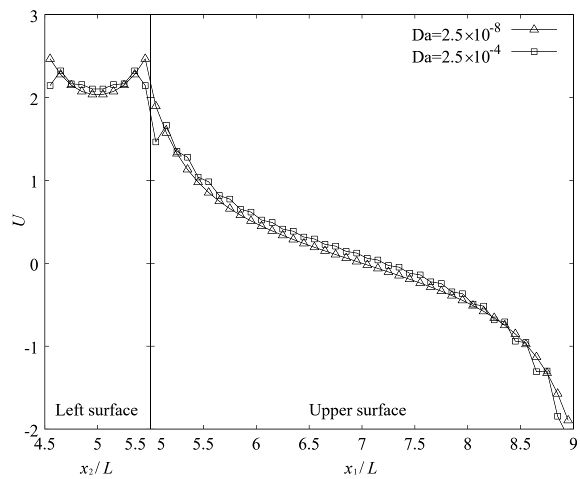

Figure 22 The in/outflow velocity on surface between void and porous medium (Aspect ratio=4.0, Re=30)

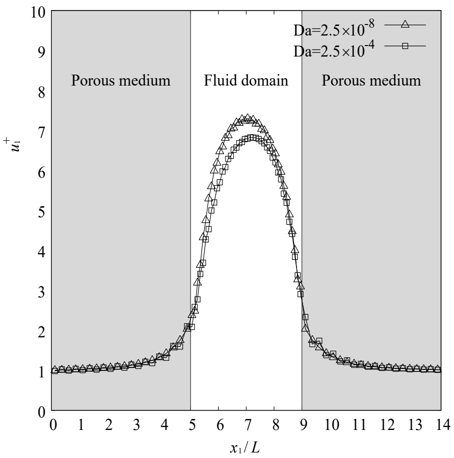

Figure 23 Distribution of horizontal velocity at x_2/L=5.0 (Aspect ratio=4.0, Re=30)

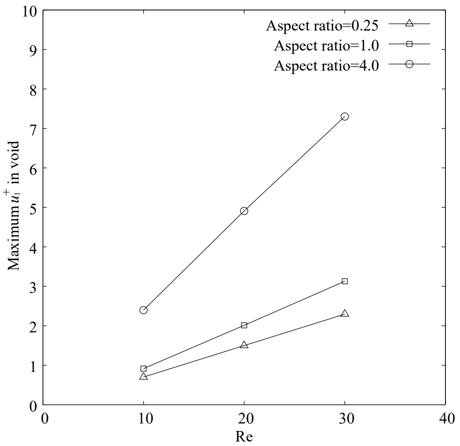

Figure 24 The relationship between maximum velocity and Re (Da=2.5×10^{-8})

5. CONCLUSIONS

This paper has presented a numerical method to achieve the simultaneous analysis of the Darcy and the Navier-Stokes flow, using the Darcy-Brinkman equations as the governing equations. The Darcy-Brinkman equations are identical to the Navier-Stokes equations when the porosity of 1.0 and the infinite hydraulic conductivity are given, and it has been shown that the Darcy-Brinkman equations can approximately satisfy the Darcy's law in porous media.

The presented numerical method was applied to the two problems; one is the backward-facing step flow with a porous step, and the other is the seepage flow around the void in a porous medium. The conclusions obtained from the numerical analyses are as follows;

1. The reattachment point do not significantly changes even if step is porous in the Backward-facing step flow analysis. However, the reattachment point slightly moves away from the step in the case of Da=1.0×10^{-3}, because the profile of the flow velocity at the edge of the step diverts from the Hagen-Poiseuille flow.
2. The shape of voids in porous media has a strong influence on the flow in it. When the shape of the void is wide and short in the flow direction, the seepage water comes into the void from the corners of its upstream side, and forms the two major streams along the upper and lower side. On the other hand, when the shape is narrow and long in the flow direction, the two streams in the upstream side combine immediately and develop into one main stream.
3. The Darcy number influences the flow velocity in the void because of the inflow and the outflow through the interface between the fluid domain and the porous medium.

6. REFERENCES

Badea, L., Discacciati, M. and Quarteroni, A. (2010) : Numerical analysis of the Navier–Stokes/Darcy coupling, Numerische Mathematik, 115, 195–227.

Bars, M.L. and Worster, M.G. (2006) : Interfacial conditions between a pure fluid and a porous medium: implications for binary alloy solidification, Journal of Fluid Mechanics, 550, 149–173.

Beavers, G.S. and Joseph, D.D. (1967) : Boundary conditions at a naturally permeable wall, Journal of Fluid Mechanics, 30(1), 197–207.

Cai, M., Mu, M. and Xu, J. (2009) : Numerical solution to a mixed Navier–Stokes/Darcy model by the two-grid approach, SIAM Journal on Numerical Analysis, 47(5), 3325–3338.

Chan, T.F., Gallopoulos, E., Simoncini, V., Szeto, T. and Tong, C.H. (1994) : A quasi-minimal residual variant of the Bi-CGStab algorithm for nonsymmetric systems, SIAM Journal on Scientific Computing, 15(2), 338–347.

Chidyagwai, P. and Rivière, B. (2009) : On the solution of the coupled Navier–Stokes and Darcy equations, Computer Methods in Applied Mechanics and Engineering, 198, 3806–3820.

Chidyagwai, P. and Rivière, B. (2011) : A two-grid method for coupled free flow with porous media flow, Advances in Water Resources, 34, 1113–1123.

Çeşmelioğlu, A. and Rivière, B. (2012) : Existence of a weak solution for the fully coupled Navier–Stokes/Darcy-transport problem, Journal of Differential Equations, 252, 4138–4175.

Fujisawa, K., Arimoto, S. and Murakami, A. (2013) : Simultaneous computation of incompressible and Darcy flows solving the Darcy-Brinkman equations, Irrigation, Drainage and Rural Engineering Journal, 287, 35-44. (In Japanese)

Girault, V. and Rivière, B. (2009) : DG approximation of coupled Navier-Stokes and Darcy equations by Beaver-Joseph-Saffman interface condition, SIAM Journal on Numerical Analysis, 47(3), 2052–2089.

Kim, D. and Choi, H. (2000) : A second-order time-accurate finite volume method for unsteady incompressible flow on hybrid unstructured grids, Journal of Computational Physics, 162, 411–428.

Kim, J. and Moin, P. (1985) : Application of a fractional-step method to incompressible Navier–Stokes equations, Journal of Computational Physics, 59, 308–323.

Liu, H., Patil, P.R. and Narusawa, U. (2007) : On Darcy–Brinkman equation: viscous flow between two parallel plates packed with regular square arrays of cylinders, Entropy, 9(3), 118–131.

Mu, M. and Xu, J. (2007) : A two-grid method of a mixed Stokes-Darcy model for coupling fluid flow with porous media flow, SIAM Journal on Numerical Analysis, 45(5), 1801–1813.

Neale, G. and Nader, W. (1974) : Practical significance of Brinkman's extension of Darcy's law: Coupled parallel flows within a channel and a bounding porous medium, The Canadian Journal of Chemical Engineering, 52, 475–478.

Ochoa-Tapia, J. and Whitaker, S. (1995a) : Momentum transfer at the boundary between a porous medium and a homogeneous fluid: I. theoretical development, International Journal of Heat and Mass Transfer, 38, 2635–2646.

Ochoa-Tapia, J. and Whitaker, S. (1995b) : Momentum transfer at the boundary between a porous medium and a homogeneous fluid: II. comparison with experiment, International Journal of Heat and Mass Transfer, 38, 2647–2655.

Saffman, P.G. (1971) : On the boundary condition at the surface of a porous medium, Studies in Applied Mathematics, 50, 93–101.

APPENDIX

Appendix A: Interpolation of velocity and pressure

The pressure and the velocity at the surface of the finite volume cells are need when calculating line integral in Eq. (19) to (22). These quantities are interpolated using the pressure and the velocity at the centroids of neighboring cells. The interpolation scheme plays very important role to solve the coupled analysis of Darcy and Navier-Stokes flows stably. Fujisawa et al. (2013) proposed the interpolation scheme which can avoid the physically unrealistic oscillation at the interface between the Fluid and the Darcy Phase. The proposed equations to interpolate the pressure, the velocity and their directional derivative at the surface of the finite volume cells are following form;

$$p_f = \begin{cases} \dfrac{\delta_b p_a + \delta_a p_b}{\delta_a + \delta_b} & \text{if both are the same phase} \\ p_a & \text{if left is fluid pahse and right is Darcy phase} \\ p_b & \text{if left is Darcy pahse and right is fluid phase} \end{cases} \tag{25}$$

$$u_{i,f} = \begin{cases} \dfrac{\delta_b u_{i,a} + \delta_a u_{i,b}}{\delta_a + \delta_b} & \text{if both are the same phase} \\ u_{i,b} & \text{if left is fluid and right is Darcy phase} \\ u_{i,a} & \text{if left is Darcy and right is fluid phase} \end{cases} \tag{26}$$

$$\left.\frac{\partial p}{\partial n}\right|_a = \begin{cases} \dfrac{p_b - p_a}{\delta_a + \delta_b} & \text{if both are the same phase} \\ \dfrac{p_b - p_a}{\delta_b} & \text{if left is fluid and right is Darcy phase} \\ \dfrac{p_b - p_a}{\delta_a} & \text{if left is Darcy and right is fluid phase} \end{cases} \tag{27a}$$

$$\left.\frac{\partial p}{\partial n}\right|_b = \begin{cases} \dfrac{p_a - p_b}{\delta_a + \delta_b} & \text{if both are the same phase} \\ \dfrac{p_a - p_b}{\delta_b} & \text{if left is fluid and right is Darcy phase} \\ \dfrac{p_a - p_b}{\delta_a} & \text{if left is Darcy and right is fluid phase} \end{cases} \tag{27b}$$

$$\left.\frac{\partial u_i}{\partial n}\right|_a = \frac{u_{i,f} - u_{i,a}}{\delta_a} \tag{28a}$$

$$\left.\frac{\partial u_i}{\partial n}\right|_b = \frac{u_{i,f} - u_{i,b}}{\delta_b} \tag{29b}$$

where p_f and $u_{i,f}$ denote the values of the pressure and the velocity at the interface, respectively, and δ is the distance from the cell centre to the interface. The subscripts a and b indicate that the values are related to the left and right cells, respectively, as seen in Figure 25 and 26. Eq. (26) is also applied to the interpolation of the intermediate velocities u_i', $\hat{u}_i$ and u_i^*.

Figure 25 and 26 illustrate the interpolation of the pressure and the velocity, respectively, when the left is the Darcy phase and the right is the fluid domain. Eq. (25) implies that the pressure is linearly interpolated if the neighboring cells are within the same phase, but that the pressure of the fluid domain is extended to the interface if the phases of the two cells are different. On the other hand, the velocity of the Darcy phase is extended to the interface if it is shared by the different phases, as described by Eq. (26). Since Eq. (25) to (28) represent the interpolation method taking the interface between the horizontally-placed left and right cells as an example, these equations are obviously applicable to any interface, such as the one between the vertically-placed upper and lower cells.

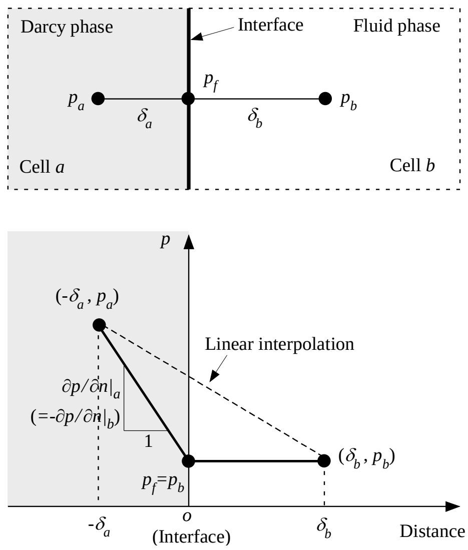

Figure 25 Interpolation of pressure at the interface between the Darcy and the fluid domains.

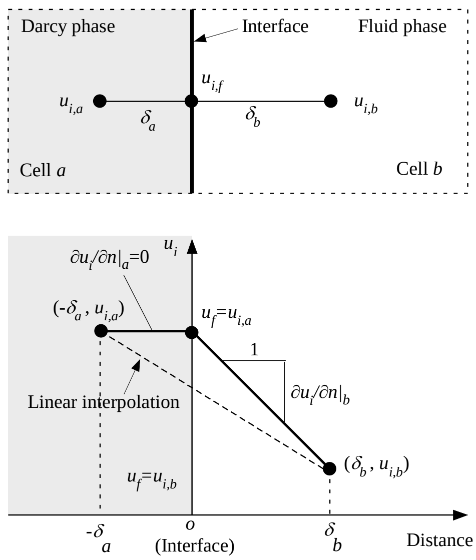

Figure 26 Interpolation of velocity at the interface between the Darcy and the fluid domains

The directional derivative of the pressure at each cell face is needed in Eq. (21) and (23). The first equality of Eq. (27) means that the directional derivative of the pressure at the interface is approximated by the linear pressure gradient between the neighboring cells when they are within the same phase. However, the second and third equalities employ the pressure gradient of the Darcy phase as the directional derivative. This is attributed to the interpolation of the velocity, i.e., Eq. (26), which extends the pressure of the Darcy phase to the interface shared by the different phases. Similarly, the porosity λ at the interface, which required by Eq. (21) and (23), is also given by the one of the Darcy phase.

It should be noted that there is the following relationship between the directional derivatives of the left and right cells;

$$\left.\frac{\partial p}{\partial n}\right|_a = -\left.\frac{\partial p}{\partial n}\right|_b \tag{29}$$

which ensures that the two fluxes of U_a^{m+1} and U_b^{m+1} calculated from Eq. (23) satisfy the following equality;

$$U_a^{m+1} = -U_b^{m+1} \tag{30}$$

If the constraint condition of Eq. (29) is not imposed, the numerical computation may break down because the mass balance of the fluid is inconsistent. The directional derivatives of the velocity does not need to have such a constraint, so that they are simply given by Eq. (28).